Check for updates

ADVANCED MATERIALS TECHNOLOGIES
www.advmattechnol.de

Multifunctional Micro/Nanofiber Based-Dressing Patch with Healing, Protection, and Monitoring Capabilities for Advanced Wound Care

Ji-Hwan Ha, Jae Yun Kim, Dahong Kim, Junseong Ahn, Yongrok Jeong, Jiwoo Ko, Soonhyoung Hwang, Sohee Jeon, Young Jung, Jimin Gu, Hyeonseok Han, Jungrak Choi, Gihun Lee, Moonjeong Bok, Su A Park, Yee Sook Cho, Jun-Ho Jeong, and Inkyu Park**

Considerable efforts have been devoted to developing wound dressings with various functions, including rapid cell proliferation, protection against infection, and wound state monitoring to minimize severe pain and the risks of wound-caused secondary infections. However, it remains challenging to diagnose wound conditions and achieve integration of the above functions without specialized equipment and expertise in wound care. This study describes an electrospun composite micro/nanofiber-based bilayer-dressing patch comprising a healing-support layer (hyaluronic acid, gelatin, and dexpanthenol) and a protective/monitoring layer (curcumin and polycaprolactone). The improved cell regeneration function and biocompatibility of the healing-support layer enable rapid healing, as evidenced by the expedited growth of fibroblasts. The superior antimicrobial properties (against *Escherichia coli* and *Staphylococcus aureus*) and visible color changes within the pH range of wound lesions (pH 6–9) of the protective/monitoring layer make the dressing suitable for advanced wound care. The wounds inflicted on BALB/c mice heal rapidly (12 days) without scars while the wound state can be diagnosed by the change in color of the dressing patch. The multifunctional wound dressing patch developed in this study is expected to promote wound healing and monitor wound state; thus, facilitating convenient wound management.

1. Introduction

Everyone can experience various wounds with different levels of severity, such as superficial wounds, burns, or ulcers. Neglecting proper care causes wounds to become severe, possibly necessitating follow-up surgery due to a myriad of factors, including formation of exudates or harmful gases and development of secondary infections.[1] These severe complications exacerbate patient discomfort and increase the required recovery time as well as the related financial expenses. Hence, researchers have continued to investigate strategies to design wound dressings that enable swift and steady recovery. Moreover, development of wound dressings that allow for simple visual monitoring of wound healing state would lessen the needs for repeated diagnoses that can expose patients to external sources of infection and the risk of developing additional wounds.

J.-H. Ha, J. Ahn, Y. Jeong, J. Ko, Y. Jung, J. Gu, H. Han, J. Choi, G. Lee, I. Park
Department of Mechanical Engineering
Korea Advanced Institute of Science and Technology
Daejeon 34141, Republic of Korea
E-mail: inkyu@kaist.ac.kr

J.-H. Ha, J. Ahn, Y. Jeong, J. Ko, S. Hwang, S. Jeon, M. Bok, J.-H. Jeong
Department of Nano-manufacturing Technology
Korea Institute of Machinery and Materials
Daejeon 34103, Republic of Korea
E-mail: jhjeong@kimm.re.kr

J. Y. Kim, Y. S. Cho
Stem Cell Research Laboratory
Immunotherapy Research Center
Korea Research Institute of Bioscience and Biotechnology
Daejeon 34141, Republic of Korea

J. Y. Kim, Y. S. Cho
Department of Bioscience
KRIBB School
University of Science and Technology
Daejeon 34113, Republic of Korea

D. Kim
Department of Applied Bioengineering
Graduate School of Convergence Science and Technology
Seoul National University
Seoul 08826, Republic of Korea

S. A. Park
Nano Convergence & Manufacturing Systems
Korea Institute of Machinery and Materials
Daejeon 34103, Republic of Korea

The ORCID identification number(s) for the author(s) of this article can be found under https://doi.org/10.1002/admt.202201765.

DOI: 10.1002/admt.202201765

© 2023 Wiley-VCH GmbH

The most common wound dressing method involves utilizing gauze as well as bandages and provides only basic wound protection features, such as protecting the wound from external sources of infection and maintaining the moisture within the wound.[2] However, as this method does not include wound-healing aids or drugs, it is unable to improve the healing speed. In addition, multi-layered bandages limit ventilation, thereby hindering the healing process. Therefore, as means to achieve rapid wound healing, researchers developed wound dressing methods based on biopolymers and bio-composite that assist in cell regeneration.[2–6] The materials, wound healing times, and other functions of previous research on functional dressings are classified in Table S1 (Supporting Information). According to the previous studies, numerous dressings currently in use provide antibacterial properties for rapid wound healing and wound protection. A dressing patch with pH sensing capabilities has also been developed, but there are limits since pH sensing of the previous wound dressings needs an additional measurement equipment or the material employed is not entirely biocompatible.[7–10] Although numerous materials were associated with improved wound healing, it is not realistic to expect a single substance to perform several beneficial roles. It is therefore important to select base materials capable of encouraging healing activities while fabricating an appropriate composite to enable targeted functions. Furthermore, efforts have been made to increase the wettability and absorption of exudates by employing hydrogels, foam rubbers, sponges, and fiber-based sheet in wound dressings.[11–13] Although progress has been made in terms of improving the basic functions of wound dressings, important features such as rapid cell regenerability, antimicrobial properties, and wound-monitoring capabilities are limited.

Advanced wound dressings should provide wound protection. Attempts to prevent wound infections from external sources such as microbial species and pollution, have been reported.[14–16] In particular, the low surface energy of wound dressings based on microscale patterning of hydrophobic polymers can prevent the attachment and growth of microbial species.[14] Moreover, antimicrobial metal nanoparticles, such as gold, silver, and copper, have been grafted with wound dressing materials[17–20]; however, the associated toxicity of metal nanoparticles—causing DNA damage, cell cycle arrest, and apoptosis—limit their applicability.[20] As an alternative, researchers have attempted to fabricate antimicrobial biocomposites using biocompatible natural compounds that are proven to be safe for long-term human exposure. Thus, natural substances that are safe and exert antimicrobial properties, such as polyphenol-rich plant extracts, have been considered for wound dressing applications.[21]

Additionally, if wound state can be continually monitored without dressing removal, appropriate care may be provided by preventing wound worsening while also identifying the degree of healing. Current approaches require the dressing to be removed to directly assess the wound state, and subsequently replaced, which may result in further infection or wound damage. As an alternative, methods for determining wound conditions using pH have been proposed. When a wound occurs, the pH of the wound lesion initially increases from 5.5–6.5 to 8–9. However, the pH subsequently decreases as acids are released in the recovered keratin layer and skin accessory structures.[22] In light of this phenomenon, an attempt was made to develop a pH sensor to monitor the wound state; however, this method requires additional equipment to measure electric signals, and its biocompatibility is relatively poor.[23,24]

In this study, we developed a wound dressing patch, composed of micro- and nanofibers fabricated through electrospinning process, that has rapid healing, protective, and monitoring functions (Figure S1, Supporting Information). Electrospinning process can fiberize various polymers to support cell regeneration as it can integrate more functions and form a porous structure by manufacturing and stacking micro- and nanosized fibers. Moreover, nanoscale fibers have large reaction areas that can rapidly deliver agents required for wound healing. Hence, the proposed design incorporates a direct skin contacting layer comprising healing-support agents, namely, hyaluronic acid (HA), gelatin (GE), and dexpanthenol (DP) to facilitate rapid wound healing. In addition, patterned curcumin and polycaprolactone (C-PCL) microfiber layers are fabricated in the outer layer to provide wound protection and monitoring. Curcumin, a natural material, can protect wounds from microbial infection, owing to its polyphenol,[25,26] while also changing color due to the pH-dependent chromaticity features generated by chemical structural changes.[27,28] The basic characteristics of this integrated multifunctional wound dressing was further analyzed using scanning electron microscopy (SEM) and Fourier transform infrared (FTIR) spectroscopy. Furthermore, the biocompatibility and wound healing support (WHS) performance of the DP, HA, and GE composite (DHG) were confirmed through an NIH 3T3 cell culture assay. In addition, the hydrophobicity of C-PCL, as well as the antimicrobial properties against *Escherichia coli (E.coli)* and *Staphylococcus aureus (S.aureus)* were evaluated. Furthermore, the chromaticity of the curcumin-based pH colorimetric sensor was optimized, and its suitability as a wound-monitoring pH sensor was assessed. Finally, the efficacy of the manufactured wound dressing patch was evaluated in a murine wound model. Thus, for the first time, a verification of the in vivo colorimetric sensing of the pH change caused by the wound state via a curcumin-based composite was performed. The proposed multifunctional wound dressing patch is expected to provide rapid healing and diagnostic convenience for wounded patients.

2. Results and Discussion

2.1. Design of Multifunctional Wound Dressing Patch

Figure 1a presents a schematic of the electrospun wound dressing patch developed in this study. The patch consists of bilayers—WHS nanofiber layer and wound protection/monitoring (WP/M) microfiber layer. These two layers were physically bonded without using an adhesive by using the electric field direction perpendicular to the ground setting in the electric radiation process. Additionally, during the electrospinning process, the hydrophilic properties of the HA and GE improved the adhesion. Furthermore, the DHG nanofibers were accumulated on the micro-scale C-PCL fibers of the WM/P layer, thereby enabling more stable binding between these layers.

© 2023 Wiley-VCH GmbH

2365709x, 2023, 7, Downloaded from https://onlinelibrary.wiley.com/doi/10.1002/admt.202201765 by Korea Advanced Institute Of, Wiley Online Library on [10/08/2023]. See the Terms and Conditions (https://onlinelibrary.wiley.com/terms-and-conditions) on Wiley Online Library for rules of use; OA articles are governed by the applicable Creative Commons License

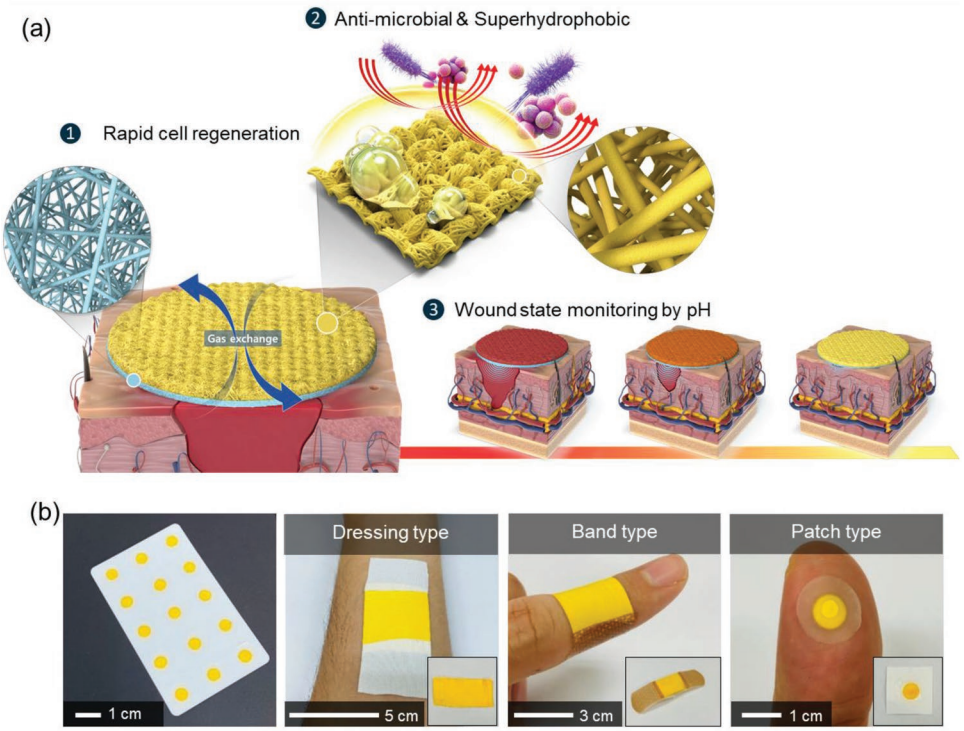


Figure 1. Schematic of the multifunctional DHG/C-PCL wound dressing patch and various prototypes. a) The multifunctional wound dressing patch consists of two layers: a DHG layer and a C-PCL layer and comprises of micro- and nanoscale fibers generated through electrospinning process. 1) For wound healing with rapid cell regeneration, nanoscale fibers in a DHG layer were fabricated to promote extracellular matrix formation and regeneration of fibroblast cells. 2) The C-PCL layer has high water repellency and antimicrobial properties due to the inclusion of rectangular mesh patterns and microscale fiber strands on the surface as well as the low surface energy of the PCL. Furthermore, the numerous polyphenol groups in the curcumin from C-PCL can increase the resistance to bacteria and effectively protect wounds from external infection. 3) The curcumin-based C-PCL is designed to monitor the wound condition as it turns red in environments with pH > 7 due to keto-enol tautomerism. b) The multifunctional wound dressing patch can be packaged in desired sizes and shapes for user convenience, and mass production is possible. Various types of wound treatments (dressings, bands, and patches) suitable for the size of the lesion can be applied.

To enhance wound healing, the WHS layer contains HA, GE, and DP (Figure 1a-1), which have been reported to promote cell regeneration by providing a biocompatible and appropriate environment.[29–31] More specifically, HA is a biocompatible material that affects extracellular matrix production and cell adhesion qualities by interacting with HA receptors such as CD44 and hyaluronan-mediated motility receptors (RHAMM).[32,33] Such interactions induce angiogenesis through endothelial cell proliferation to enable rapid healing. GE is reportedly used frequently as a scaffold for tissue engineering and to induce superior cell interactions, including cell adhesion, stretching, and proliferation. In addition, GE exhibits high stability due to its low antigenicity and high bio-absorption rate.[30] Therefore, stable cell culture and cell settlement are promoted, resulting in stable tissue regeneration. Furthermore, owing to their superior hygroscopicity and porous structure, HA and GE can continually absorb exudate from the wound site, preventing the lesion from deteriorating. DP is a precursor of pantothenic acid (vitamin B5) and is used as a wound pharmaceutical product owing to its anti-inflammatory and cell recovery characteristics.[31] Moreover, DP can prevent scarring, help skin wounds heal rapidly, and enhance the growth rate of fibroblasts.

From a structural perspective, the layer that directly attaches to the wound consisted of numerous nanofibers fabricated through electrospinning process. Due to the large surface area of the WHS layer, nanosized electrospun composite fibers could swiftly transmit the elements and anti-inflammatory components necessary for cell growth.

In addition to the rapid wound healing, infection prevention and wound-monitoring are key factors in wound dressings. Therefore, the WP/M layer was designed using a C-PCL composite for wound protection and monitoring. The base materials, PCL and curcumin, are biocompatible, superhydrophobic, and antimicrobial due to their low surface energies (Figure 1a-2). In addition, these functions may be improved by the surface patterning (e.g., a mesh pattern of hundreds of micrometers) of the WP/M layer. Curcumin is a natural material with numerous polyphenolic groups. Consequently, curcumin-based composites exhibit antimicrobial and antioxidant properties.[32] Moreover, it enables the identification of the wound state based on the color change in response to pH variation (Figure 1a-3). The colorimetric sensing function of the patch can help patients self-diagnose their wound states.

Furthermore, the two layers of the wound care system can exchange gases generated at the lesion due to the high gas permeability of the electrospun micro- and nanoscale fiber mats. We fabricated various prototypes of dressings, bands, and patches, as shown in Figure 1b. Electrospun wound

© 2023 Wiley-VCH GmbH

2365709x, 2023, 7, Downloaded from https://onlinelibrary.wiley.com/doi/10.1002/admt.202201765 by Korea Advanced Institute Of, Wiley Online Library on [10/08/2023]. See the Terms and Conditions (https://onlinelibrary.wiley.com/terms-and-conditions) on Wiley Online Library for rules of use; OA articles are governed by the applicable Creative Commons License

dressing patches are flexible and can be cut into arbitrary forms depending on the wound size.

2.2. Biocompatible DHG Layer Facilitates Rapid Wound Healing

We fabricated a nanofiber layer by mixing HA, GE, and DP, compounds with excellent wound regeneration effects (**Figure 2**a). Previous studies have shown that HA can promote rapid healing by supporting cells during wound healing through interactions with certain surface receptors, collagen deposition, and angiogenesis. Although attempts have been made to scale down HA using electrospinning process and enhance its reactivity, it has been reported that the fabrication of nanoscale HA is problematic for several reasons.[33] For instance, due to the high viscosity and surface tension of the HA aqueous solution, which limit the maximum concentration during the electrospinning process, it is difficult for pure HA to form nanoscale fibers through electrospinning process. Furthermore, the preservation of the resultant nanofibers is hampered by their weak polymeric chains and high wettability. Meanwhile, electrospun pure HA causes HA nanofibers to coalescence. Therefore, GE, comprising a strong polymer chain, was added to form and maintain stable HA-based nanofibers, as well as enhance cell regeneration. Consequently, the binding force between the polymer chains was improved

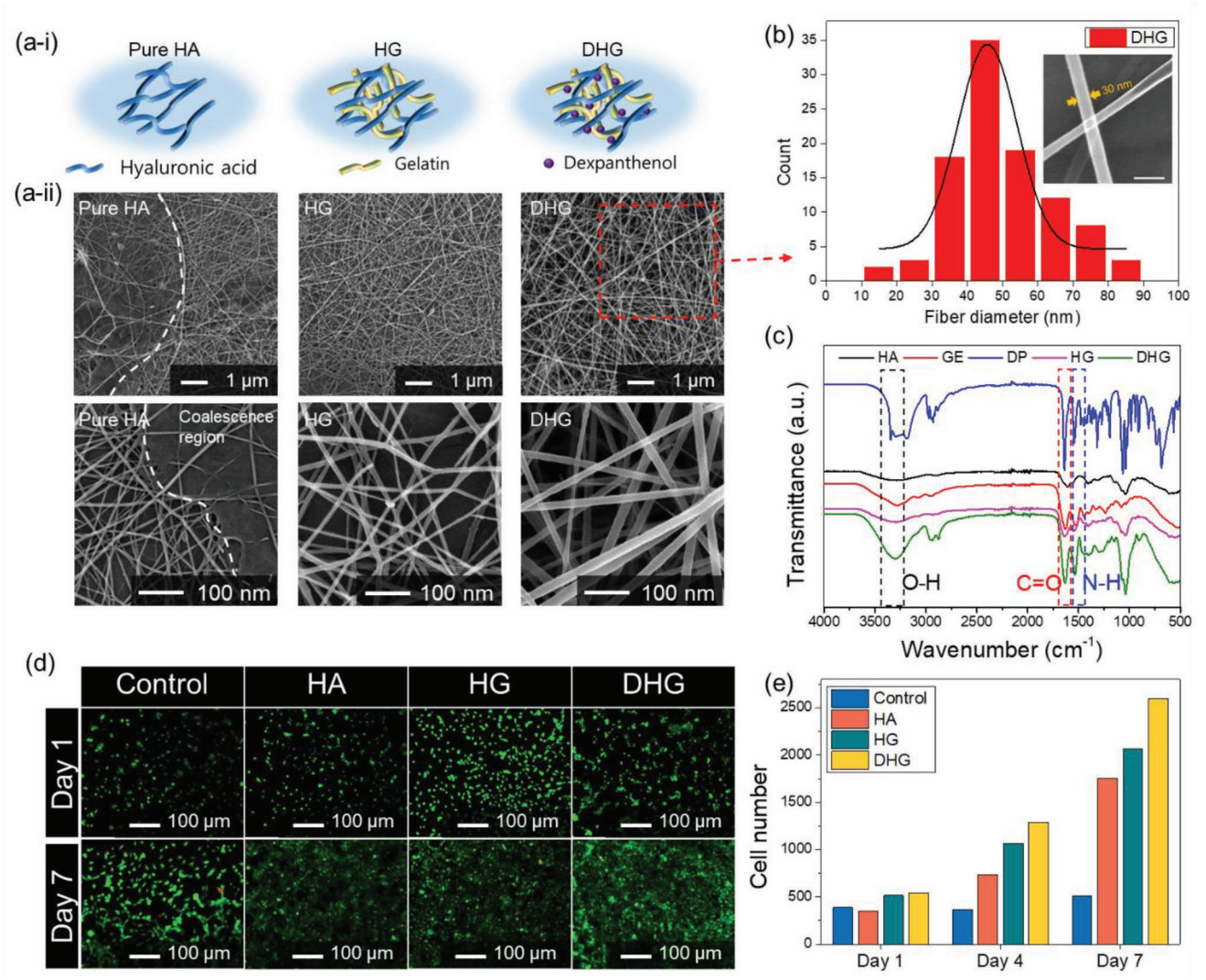


Figure 2. Design and characterization of the WHS layer composed of DHG for biocompatibility and wound healing. a) Schematic of i) HA, HG, and DHG and ii) SEM images of each nanofiber (HA, HG, and DHG) fabricated through electrospinning process. Although nanofibers that are unstable and prone to coalescence are fabricated due to the weak polymer chain of pure HA, the composite with GE has improved nanofiber maintenance properties due to the strong polymer chain of GE. Based on the complemented HG composite, DHG containing DP drugs with fibroblast cell promotion effects was finally developed. b) Diameters of DHG fibers are distributed from 10 to 90 nm. High resolution SEM image of DHG nanofiber (scale bar: 100 nm). c) FTIR analysis results for each component and composite: HA, GE, DP, HG, and DHG. The number of functional groups per unit volume in the OH group as well as amide I and II groups increased in the DHG composite. d) Live and dead NIH 3T3 cell viability assay of control (PET), HA, HG, and DHG over 7 days (green: live cell, red: dead cell). e) The live cell number of each experimental group was measured using an image processing tool (Image J).

© 2023 Wiley-VCH GmbH

2365709x, 2023, 7, Downloaded from https://onlinelibrary.wiley.com/doi/10.1002/admt.202201765 by Korea Advanced Institute Of, Wiley Online Library on [10/08/2023]. See the Terms and Conditions (https://onlinelibrary.wiley.com/terms-and-conditions) on Wiley Online Library for rules of use; OA articles are governed by the applicable Creative Commons License

2365709x, 2023, 7, Downloaded from https://onlinelibrary.wiley.com/doi/10.1002/admt.202201765 by Korea Advanced Institute Of, Wiley Online Library on [10/08/2023]. See the Terms and Conditions (https://onlinelibrary.wiley.com/terms-and-conditions) on Wiley Online Library for rules of use; OA articles are governed by the applicable Creative Commons License

(Figure 2a-i) and stable composite nanofibers were formed, as shown in the SEM image in Figure 2a-ii.

The nanofiber structure at different HA:GE ratios (weight ratio of HA to GE = 1:0, 1:0.3, 1:0.5, and 1:1) was observed using SEM. Results show that fabrication of the fibers with a HA:GE = 1:1 prevented coalescence (Figure S2, Supporting Information). Subsequently, the DP composite (DHG) was added to the dressing to improve the rate of wound healing. The diameters of the DHG nanofibers were distributed between 10 and 90 nm (mean: 50 nm, standard deviation: 14.4 nm; Figure 2b). Figure 2c shows the verification of each component and composite incorporation by FTIR analysis. Hydroxyl groups were observed in HA, GE, and DP, with DP having the most functional groups per unit volume. Due to the increase in hydroxyl groups, the DHG peak, including all three materials, increased more than those of HA and GE (3200 cm^{-1}). In addition, the results confirmed that the three materials were mixed well, as evidenced by the increase in the amide I (1650 cm^{-1}) and amide II (1540 cm^{-1}) peaks due to the inclusion of GE and DP. Cell growth assays were performed for 7 days to confirm the biocompatibility and degree of fibroblast cell culture characteristics on the WHS layer. Figure 2d shows the fluorescence images of NIH 3T3 cells grown on a bare PET substrate (control) and PET substrates with HA, HG, and DHG nanofibers after 1 and 7 days (Figure S3, Supporting Information). Consequently, the cell culture growth occurred in the order of DHG > HG > HA > bare PET substrates (Figure 2e). These results verified that HA nanofibers effectively induced cell growth due to the interaction between HA, CD44, and RHAMM receptors, while the cell growth rate was also markedly increased due to the protein provision of GE. Finally, compared to pure HA, the superior fibroblast cell regeneration activity of DP increased the cell culture features of the composites containing DP. Furthermore, the DP is continuously released over time (Figure S4, Supporting Information). For 12 h, the DP cumulative drug release rate is increased from 0% (at 0 h) to 46.7% (after 0.5 h), and to 98.5% (after 12 h). According to the cell proliferation test results, DHG nanofiber layer shows the best cell proliferation rate, and this can be attributed to the continuous drug release. Consequently, DHG, exhibited excellent biocompatibility and cell regeneration effects likely owing to the synergy of each element contributing to rapid wound healing. Therefore, these components are suitable for use in WHS layers to facilitate rapid healing through direct contact with wounds.

2.3. Wound Protection Performance of the WP/M Layer

We fabricated a C-PCL outer layer, the WP/M layer, to prevent contamination from external sources, such as germs and microbial species. In **Figure 3**a, the morphological differences are shown in SEM images of the C-PCL/DHG composite dressing patch. Unlike nanoscale DHG fibers, the C-PCL fibers have microscale diameters (diameters of 1–2 µm, Figure S5, Supporting Information). The WP/M layer was likely

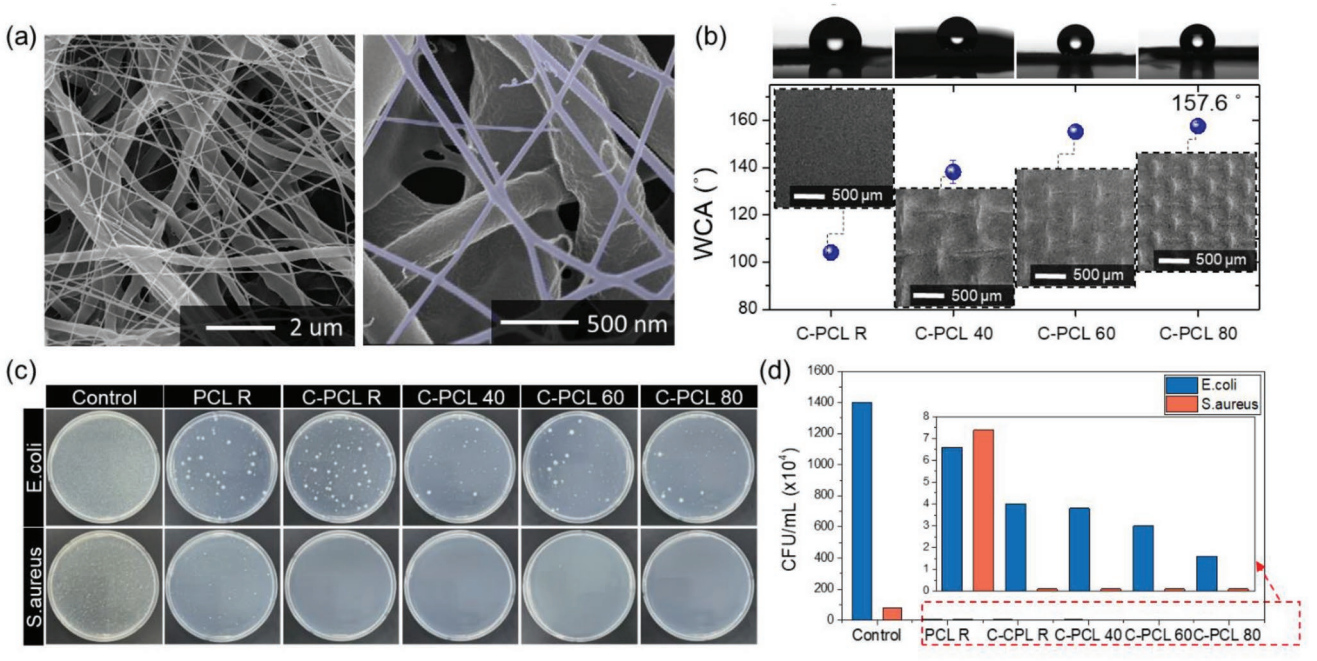


Figure 3. Protection performance of the WP/M layer composed of C-PCL. a) Surface morphology of the C-PCL/DHG wound healing patch. The diameters of the C-PCL and DHG fibers (blue color) are on a microscale (1–2 µm) and nanoscale (30–60 nm), respectively. b) The water contact angles (WCAs) of C-PCL R, 40, 60, and 80 were measured. The inset images show the morphological characteristics of each sample. As the spacing of the C-PCL square mesh narrows, the hydrophobicity improves due to increased pattern density and height influence. The highest water repellency angle is observed for C-PCL 80 at 157.6°. c) Antimicrobial performances of PCL (random) and C-PCL (random, 40, 60, and 80) against *E. coli* and *S. aureus* for 14 days. d) The number of colony-forming units was counted for each sample. A low surface energy and PCL patterns inhibit the adsorption and growth of bacteria, and antimicrobial enhancement due to polyphenols of curcumin shows maximum antimicrobial properties in C-PCL 80.

 © 2023 Wiley-VCH GmbH

superhydrophobic (water contact angle, $\theta_w > 150°$) due to the low surface energies of the materials, micronization of the fiber scale associated with electrospinning process, and formation of a micropattern (e.g., square mesh). We classified C-PCL random (C-PCL R), C-PCL 40 (hole size, 460 μm), C-PCL 60 (280 μm), and C-PCL 80 (150 μm) according to the square mesh patterns. The hydrophobicity generally increased with higher micropattern density (Figure 3b). Hydrophobicity depends on the roughness and shape of the surface, as described by Wenzel[34] [$\cos(\theta) = r\cos(\theta Y)$] and Cassie–Baxter[35] [$\cos(\theta) = \varphi s(\cos(\theta Y) + 1) - 1$].[36] The Wenzel model reflects the roughness of a solid surface with water droplets completely covering the surface. Alternatively, the Cassie–Baxter model was defined to be applicable to porous surfaces by expanding the Wenzel model. Electrospun C-PCL R composed of microfibers rather than flat C-PCL films showed improved hydrophobicity due to the high surface roughness and porosity. The square mesh patterned C-PCL corresponds to the Cassie–Baxter model, in which water cannot fill the grooves of rough solids due to the high porosity, microscale pattern spacing/height, and fiber-related roughness. Accordingly, the high pattern density of C-PCL 80 exhibits a water contact angle of 157.6°.

The pattern morphologies of the C-PCL were analyzed using a laser confocal microscope (Figure S6, Supporting Information). These results indicated that the heights of the protruding mesh patterns were 195 μm (C-PCL 40), 144 μm (C-PCL 60), and 82.2 μm (C-PCL 80), and the density of the protruding regions improved with increasing density of the mesh intervals. Furthermore, antimicrobial assays (JIS Z 2801 standard test method) were conducted with *E. coli* and *S. aureus* to verify the ability of C-PCL to protect wounds. The pure PCL random (PCL R) layer prevented the adsorption of microbes, compared to the control (nutrient agar plate), owing to the low surface energy of the rough PCL layer (Figure 3c). The antimicrobial performance of the C-PCL R layer markedly reduced microbial growth due to the action of the curcumin polyphenol (*E. coli*: 39%, *S. aureus*: 98% compared to PCL R). Furthermore, denser micropatterns improved the antimicrobial properties by reducing microbial adsorption. That is, the C-PCL reduced the gram-negative *E. coli* (Table S2, Supporting Information) number from 1.4×10^7 CFU mL^{-1} (control) to 1.6×10^4 CFU mL^{-1} (C-PCL 80; Figure 3d), whereas that of gram-positive *S. aureus* (Table S3, Supporting Information) was reduced from 7.7×10^5 CFU mL^{-1} (control) to below 10 CFU mL^{-1} (C-PCL 80).

2.4. Colorimetric Sensing Performance of WM/P Layer for Wound State Monitoring

C-PCL can be used as a colorimetric pH sensor via chemical changes of curcumin and enol-keto tautomerization (**Figure 4**a). Therefore, under basic conditions, the WP/M layer changes from yellow to red due to the H-atom transfer of curcumin at an increased pH (>7). Curcumin exists in a neutral form (H3A), H2A-, HA2-, and A3- at pH 1–7, pH 7–8, pH 8.5, and pH >9, respectively. We observed the pH detection performance according to curcumin content (5, 10, 20, and 30 wt%) to improve the base detection sensitivity of curcumin (Figures S7 and S8, Supporting Information). A 30 wt% C-PCL composite with the most sensitive color change was selected, as a clear color classification under pH 7–9 conditions was required to monitor the wound condition. When the pH 9 buffer solution was applied, the C-PCL changed to red within 30 s. After applying a pH 6 buffer solution, the color changed from red to yellow, which is its original color (Figure S9, Supporting Information). The FTIR analysis results illustrated in Figure 4b demonstrate that the peaks of aromatic C = C stretching (1625 cm^{-1}) and O–H stretching (3504 cm^{-1}) tended to decrease due to changes in the curcumin chemical structure under basic conditions (pH 13). As shown in Figure 4c, color variation was observed for a wider range of pH conditions (pH 4, 7, 10, and 13) to evaluate the pH-sensing performance. When using the CIE 1931 color space to depict the color variation of C-PCL according to pH, it can be seen that the color changed from yellow to red as the pH increased (Figure 4d). The decrease in the red (R) and green (G) values and the increase in the blue (B) values are shown in Figure 4e. It is particularly suitable for wound-monitoring applications based on chromaticity differences as the variations in the R and G values are significant within the range in which pH changes during wound healing.

2.5. In Vivo Wound Healing Performance of Multi-Layer Dressing Patch

We employed a murine excisional wound healing model to verify the practical wound healing, protection, and monitoring effects of the final C-PCL/DHG multilayer patch. Patches of various circular configurations (control, non-permeable DHG, only C-PCL, C-PCL/HA, C-PCL/HA, and C-PCL/DHG) were used (**Figure 5**a). To measure the effectiveness of the patches in each group, the wound size was observed for 12 days after patch application, as shown in Figure 5b. The patches were secured without any additional treatment during the experimental period. Macroscopic assessment of the wound size from images taken at days 0, 2, 5, 8, and 12 of healing (Figure 5c) indicated that the average wound area was significantly reduced in the wounds treated with C-PCL/DHG patches on days 5 (59.49%) and 8 (82.41%). On day 1 of the experiment, the wound sizes in all groups were similar (wound area, 28 mm^2). On day 5, scabs formed on the wounds of each group, and the wound size began to decrease. On day 8, the C-PCL/DHG group exhibited superior healing compared to all other groups. The wounds treated with the C-PCL/DHG patch became more homogeneous and consistent in texture. By day 12, the wounds treated with C-PCL/DHG patches had nearly healed, confirming the superior wound healing effects of C-PCL/DHG.

Furthermore, the importance of the continuous exchange of harmful gas from the lesions with fresh air was verified using electrospun DHG patches covered with a PET film that inhibited gas permeation. On the other hand, the air permeability of C-PCL/DHG is 78.7 L m^{-2} s^{-1} (Figure S10, Supporting Information). This result means that the C-PCL/DHG dressing patch can continuously circulate harmful gases generated in the wound region. Consequently, non-permeable DHG patches

© 2023 Wiley-VCH GmbH

2365709x, 2023, 7, Downloaded from https://onlinelibrary.wiley.com/doi/10.1002/admt.202201765 by Korea Advanced Institute Of, Wiley Online Library on [10/08/2023]. See the Terms and Conditions (https://onlinelibrary.wiley.com/terms-and-conditions) on Wiley Online Library for rules of use; OA articles are governed by the applicable Creative Commons License

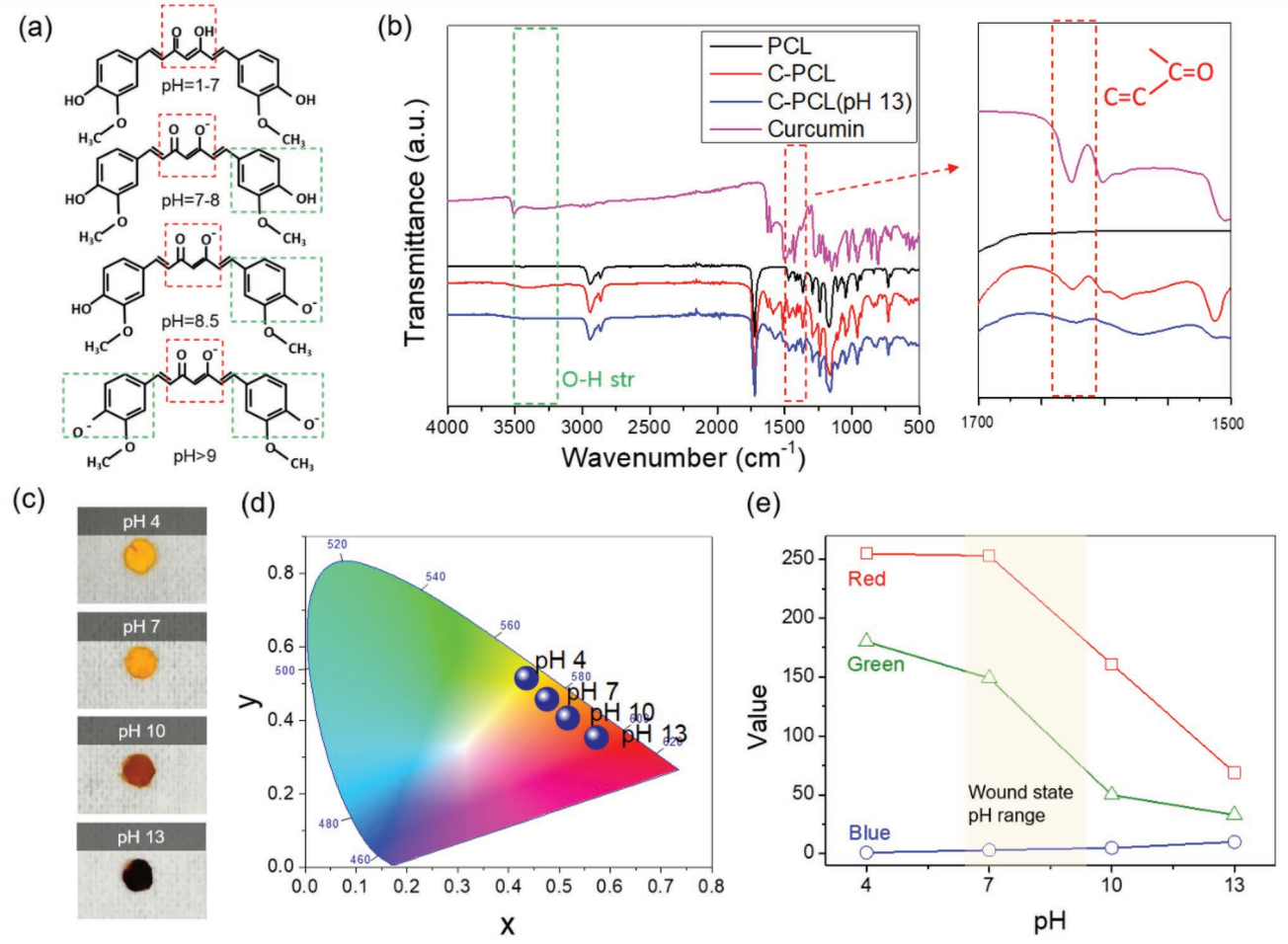


Figure 4. Colorimetric sensing performance of the WP/M layer (C-PCL) based on pH values for wound state monitoring. a) The chemical structure of curcumin changes with pH by enol-keto tautomerism. Changes in the chemical structure of curcumin in environments over a pH 7 result in color changes in the curcumin-based composites (pH = 1–7; H3A, pH = 7–8; H2A-, pH = 8.5 HA2-, pH > 9; A3-). b) Verification of the chemical structure variation via FTIR analysis (green: O–H stretching, red: aromatic moiety C = C stretching). Although curcumin increases the O–H and C = C stretching, at pH 13, the peak decreases due to loss of phenol groups following changes in the chemical structure. c) C-PCL color variation according to pH (pH 4: yellow, pH 7: orange, pH 10: red, pH 13: brown). d) Color of C-PCL according to pH on the CIE 1931 color space. e) RGB values of the C-PCL for pH 4–13.

hindered gas exchange in the lesion, slowing the wound healing progress, and impeding homogenously healing within 12 days. The pure C-PCL patches, which enabled gas permeation of lesions, but did not contain cell regeneration layers (DHG), also resulted in incomplete wound recovery within 12 days. The patches containing C-PCL, HA, or HG rapidly reduced the wound size owing to cell regeneration and wound protection performance; however, they yielded reduced wound healing performance compared to those containing C-PCL/DHG. Thus, wound healing occurred most readily when the promotion of cell regeneration, exudate absorption, gas permeation, and wound protection (antimicrobial and superhydrophobic properties) were all fulfilled.

The occurrence of an initial wound increased the pH of the wound site causing the color of the attached dressing patch to clearly change to red (Figure 5d). As the wound healed, the patch color changed from red to orange and finally to yellow owing to the pH decrease. The distinct color change of the patch with the change in the pH might indicate the state of the affected area as the entire area was homogenous. The pH change pattern, according to the recovery of such wounds (red points), corresponds to the colorimetric change distribution results observed using a pH buffer solution (blue points). As the wound recovered over 12 days, the R and G values decreased, whereas the B value increased (Figure S11, Supporting Information). Moreover, analysis of the RGB values of wound dressing patches will facilitate the numerical prediction of wound pH values. These results suggest that the C-PCL/DHG patch facilitates wound healing owing to its rapid cell regeneration and protective properties, while also allowing the monitoring of wound healing progression via visible color changes. Due to its superior flexibility and mechanical stability (maximum stress: 7.3 MPa, maximum strain: 600%, yield strength: 1.73 MPa, and Young's modulus: 0.14 MPa), this wound dressing patch is easily attached to the wound region (or curved surface) and can stably maintain the shape of the dressing patch until the wound healing is completed (Figure S12, Supporting Information).

© 2023 Wiley-VCH GmbH

2365709x, 2023, 7, Downloaded from https://onlinelibrary.wiley.com/doi/10.1002/admt.202201765 by Korea Advanced Institute Of, Wiley Online Library on [10/08/2023]. See the Terms and Conditions (https://onlinelibrary.wiley.com/terms-and-conditions) on Wiley Online Library for rules of use; OA articles are governed by the applicable Creative Commons License

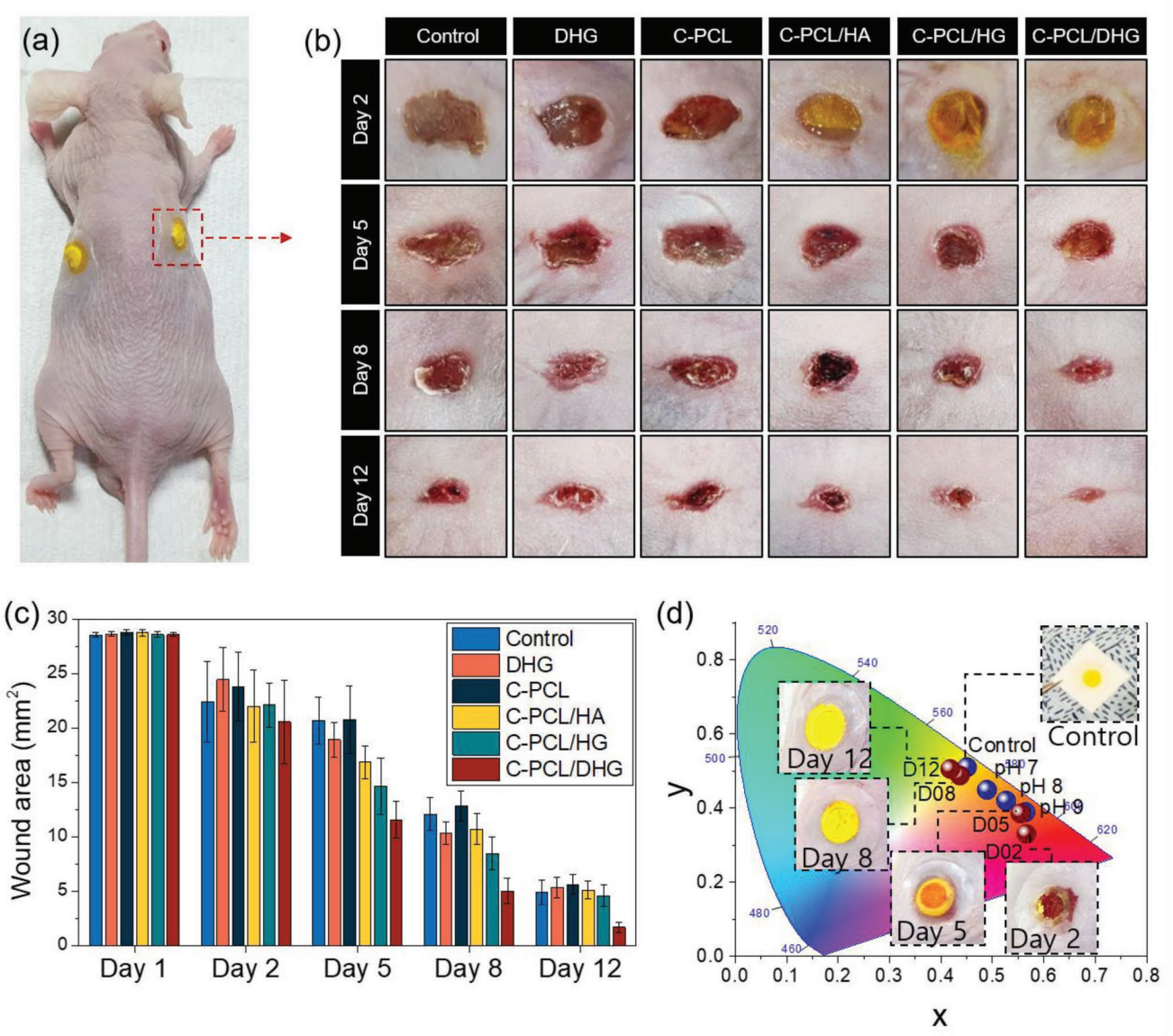


Figure 5. Wound healing and monitoring performance of the versatile bilayer wound dressing patch containing C-PCL/DHG. a) Mouse with a fabricated wound dressing patch attached. b) Comparison of the wound area recovery degree according to the wound dressing patch components over 12 days. The experiment included control, non-permeable DHG, C-PCL, C-PCL/HA, C-PCL/HG, and C-PCL/DHG groups. c) Quantitative changes in wound size measured over a 12-day period, where the C-PCL/DHG wound dressing patch provides the most rapid wound healing and protection. d) Color changes of the wound dressing patch due to the pH variation of the wound on the 1931 CIE color space. When an initial wound occurs, the color of the wound dressing patch turns red due to the increase in pH and as the wound heals over time, the color of the dressing patch changes to yellow.

3. Conclusion

In this study, an advanced versatile wound dressing capable of rapid wound healing, protection, and condition monitoring was developed. To ensure improved functionality of these aspects, the WHS nanofiber layer in direct contact with the wound was composed of HA, GE, and DP, which can rapidly proliferate cells and effectively absorb exudates from wounds. To protect wounds from outside contaminants and prevent wound deterioration, the WP/M microfiber layer was fabricated with a square mesh pattern to improve its protection performance from pollutants such as liquid and microbials. Additionally, the pH colorimetric sensing performance of C-PCL composite fiber layer proved highly suitable for monitoring the wound state owing to the wide range of color changes under basic conditions (pH > 7). The bilayers were stacked using an electrospinning process and relying on electrical field direction and adhesion forces of DHG layer without any adhesive. The manufactured wound dressing was composed of micro- and nanofibers (high porosity) to ensure gas permeability of the wound. Although studies on the improvement of each function have been reported, this research represents the integration of a multifunctional patch using natural materials. Wound dressings that integrate various functions help patients to independently

© 2023 Wiley-VCH GmbH

2365709x, 2023, 7, Downloaded from https://onlinelibrary.wiley.com/doi/10.1002/admt.202201765 by Korea Advanced Institute Of, Wiley Online Library on [10/08/2023]. See the Terms and Conditions (https://onlinelibrary.wiley.com/terms-and-conditions) on Wiley Online Library for rules of use; OA articles are governed by the applicable Creative Commons License

diagnose and manage their wounds. The superior performance of our multifunctional wound dressing patches was verified by observing the improvement in wound healing performance (rapid healing and protection) in a mouse model. Furthermore, intelligent wound state monitoring performance was verified by observing the colorimetric change of the patch according to the wound state. It is expected that the developed wound dressings can be applied to various wound situations such as skin injury, pressure ulcers, necrosis of organ tissue, and regeneration of nerve cuts through the selection of appropriate materials.

4. Experimental Section

Materials: HA (HA-TLM, 10 kDa–1.8 MDa) was purchased from Bloomage BioTechnology Co., Ltd (Beijing China). GE (type B), DP, PCL (Mw = 80 000), and curcumin were purchased from Sigma-Aldrich (St. Louis, MO, USA). Dichloromethane and dimethylformamide (DMF) were purchased from Duksan Chemical (Incheon, Korea).

Fabrication: The C-PCL/DHG fabrication scheme in Figure S1 (Supporting Information) illustrates the electrospinning process. First, HA:GE:DP (1.5 wt% each compared to the whole solution at a 1:1:1 volume ratio) was poured into DMF and stirred for 10 min. Deionized (DI) water was subsequently poured into the DHG solution and stirred for 4 h. Next, sonication dispersion was conducted for 30 min using a sonication bath. The C-PCL solution was prepared using a similar process. PCL was dissolved in dichloromethane/DMF (1:1 volume ratio) for 1 h using a magnetic stirrer. Various contents of curcumin were added to the PCL solution (5, 10, 20, and 30 wt% compared to the polymer). An additional stirring process was performed for 3 h. Next, the C-PCL solution was sonicated to homogenously disperse the curcumin. The electrospinning process was conducted using a copper mesh for C-PCL patterning; 40, 60, 80, and 100 mesh were used for various scale patterns. The C-PCL solution was injected at 1.5 mL h^{-1} with 22 kV input power and electrospinning process was performed for 30 min. After C-PCL fabrication, the DHG (or HA or HG) solution was electrospun onto the backside of the patterned C-PCL. The electrospinning process conditions were as follows: injection speed of 1.5 mL h^{-1}, input power of 25 kV, and process time of 30 min. After spinning, the patch was fabricated by cutting the C-PCL/DHG sheet into various forms. The process distance between the nozzle and target surface was 15 cm.

Characterization: Field emission scanning electron microscopy (FE-SEM, Sirion, Thermo Fisher Scientific, Inc., Waltham, MA, USA) was used to observe the morphology of the C-PCL/DHG fibers. An FTIR spectrometer (Nicolet iS50, Thermo Fisher Scientific, Inc.) was used to verify the composite components. Additionally, changes in the chemical structure of C-PCL were confirmed through FTIR spectroscopy. Basic color change experiments on C-PCL were conducted using buffer solutions (pH 4–13), which were added dropwise onto the C-PCL patch. In addition, the color of the C-PCL was observed using optical microscopy. The hydrophobicity of the C-PCL was measured using a DO4010 contact angle meter (Kruss GmbH, Hamburg, Germany). The air permeability of C-PCL/DHG dressing patch were measured by the ISO 9237 (1995) method.[35] The test area and air pressure of C-PCL/DHG composite sheet for air permeability were 20 cm^2 and 100 Pa, respectively. The mechanical properties of C-PCL/DHG was measured using a universal testing machine (UTM; AGS-X, Shimadzu). The tensile speed was 1 mm min^{-1}.

Drug Release: Dexpanthenol release experiment[36,37] was conducted using UV–visible spectrophotometer (Lambda 1050, wavelength: 210 nm) analysis. The DHG nanofiber based-layer sheet was poured to the phosphate-buffered saline (PBS) solution. The PBS solution volume was 20 mL. The dexpanthenol release time were 0.5, 1, 2, 4, 6, 9, and 12 H. The temperature of PBS solution with DHG sheet 37 °C (normal body temperature).

Cell Culture: NIH 3T3 cells were used for cell assays. Cells were cultured in Dulbecco's modified Eagle's medium (Gibco, Waltham, MA, USA) supplemented with 10% fetal bovine serum and 1% penicillin. All samples were sterilized by soaking in 70% ethanol for 1 min and washed with phosphate-buffered saline to remove the residual ethanol. Subsequently, 5×10^4 cells per sample were seeded and cultured at 37 °C in an incubator with 5% CO_2.

Cell Viability (Compatibility) Assay: A live/dead kit (LIVE/DEAD Viability/Cytotoxicity Kit; Invitrogen, Carlsbad, CA, USA) was used to investigate the viability of NIH/3T3 cells. Viability was confirmed 1 and 7 days after seeding. Cells were stained with a dying solution containing calcein-AM and ethidium homodimer-1. Live and dead cells were investigated using a fluorescence microscope (Eclipse Ti; Nikon, Japan).

Antimicrobial Test: The antimicrobial efficacy against *E. coli* and *S. aureus* was assessed according to the JIS Z 2801 standard method. A liquid culture medium (nutrient agar plate: Bacto-Peptone 5 g, beef extract 3 g, DI water 1000 mL) was used for microorganism growth. Nutrient agar was sterilized by autoclaving (103 kPa, 120 °C). The microbes were cultivated in a 10 mL nutrition agar medium at 37 ± 1 °C for 24–48 h. They were further cultivated for 18 h in a glass container with three control test specimens and three processed samples. All flat media were cultured at 37 ± 1 °C for 24–48 h, and after incubation, the colonies from a Petri dish with 30–300 colonies of probiotic water were counted and recorded. The number of live microbes (M) was calculated according to the following formula:

$$M = Z \times R \times 20 \tag{1}$$

where Z is number of colonies, R is the dilution factor, 20 is the amount of saline.

The antimicrobial reduction rates were calculated as:

$$\text{Antimicrobial reduction rates} = \log M_a - \log M_c \tag{2}$$

where M_a is the initial control live microbial number, M_c is the live microbial number after 18 h of incubation.

Animals: The present study was performed on 8-week-old male BALB/c mice purchased from Dae Han BioLink Co., Ltd. (Chungbuk, South Korea). Mice were maintained under specific pathogen-free conditions at an animal facility at the Korea Research Institute of Bioscience and Biotechnology (KRIBB) under controlled standard temperature (20–22 °C) and humidity (50–60%). All animal experiments were approved by the Institutional Animal Care and Use Committee of the KRIBB (KRIBB-AEC-21078).

Wound Healing Analysis: An excisional, full-thickness wound model was used to evaluate the effects of C-PCL/DHG on wound healing. Mice were divided into six groups (n = 3 per group) as follows: control group (no treatment), C-PCL/DHG, C-PCL/HG, C-PCL/H, DHG (non-permeability), and C-PCL-treated groups. Each circular dressing patch was attached to the edge with skin tape, and the central portion was exposed for performance evaluation. The dressing patches were replaced once a day.

Mice were anesthetized using a 2.5% 2,2,2-tribromoethanol (Sigma-Aldrich) intraperitoneal injection. Two full-thickness dermal wounds (5 mm) were created on the dorsum of each mouse using a standard biopsy punch (Integra Miltex, Davies Dr, York, PA, USA). Patches were applied to the excisional wounds immediately after wounding. The wound size of each mouse was measured on days 0, 2, 5, 8, and 12 post-surgery. The wound closure was calculated as a percentage using the following formula:

$$\text{wound closure}(\%) = \left[\left(\text{wound area on day 0} - \text{wound area on dayn}\right) / \text{wound area on day 0}\right] \times 100 \tag{3}$$

© 2023 Wiley-VCH GmbH

2365709x, 2023, 7, Downloaded from https://onlinelibrary.wiley.com/doi/10.1002/admt.202201765 by Korea Advanced Institute Of, Wiley Online Library on [10/08/2023]. See the Terms and Conditions (https://onlinelibrary.wiley.com/terms-and-conditions) on Wiley Online Library for rules of use; OA articles are governed by the applicable Creative Commons License

Supporting Information

Supporting Information is available from the Wiley Online Library or from the author.

Acknowledgements

This work was supported by a National Research Foundation of Korea (NRF) grant funded by the Korean government (MSIT, No. 2021R1A2C3008742); Center for Advanced Meta-Materials (CAMM) funded by the Ministry of Science, ICT, and Future Planning as a Global Frontier Project (CAMM No. 2014M3A6B3063707); and National Research Foundation of Korea (NRF-2019-M3A9H1103797).

Conflict of Interest

The authors declare no conflict of interest.

Author Contributions

The manuscript was written based on contributions from all authors. J.-H. Ha conducted the experiments, analyzed the data, and wrote the manuscript. J.-H. Ha, J. Ahn, Y. Jeong, J. Ko, and Y. Jung discussed the results of the multifunctional wound healing patch fabrication and bio-application. S. Hwang, S. Jeon, M. Bok, and J.-H. Jeong discussed the results of hyaluronic acid-based composite fabrication. D. Kim and S.A. Park supported the cell proliferation experiments. J.Y. Kim and Y.S. Cho performed the mice wound healing experiments. Y. Jeong, J. Gu, H. Han, G. Lee and J. Choi discussed the results of the C-PCL composite analysis. J.-H. Jeong and I. Park contributed to the overall direction of the project. All authors have approved the final version of the manuscript.

Data Availability Statement

The data that support the findings of this study are available from the corresponding author upon reasonable request.

Keywords

antimicrobial wound dressing, electrospun composite fiber, micro/nano scale fiber, multifunctional wound dressing, pH colorimetric sensible dressing

Received: October 18, 2022
Revised: December 11, 2022
Published online: February 3, 2023

[1] G. C. Gurtner, S. Werner, Y. Barrandon, M. T. Longaker, *Nature* **2008**, *453*, 314.
[2] R. Zeng, C. Lin, Z. Lin, H. Chen, W. Lu, C. Lin, H. Li, *Cell Tissue Res.*. **2018**, *374*, 217.
[3] E. Rezvani Ghomi, S. Khalili, S. Nouri Khorasani, R. Esmaeely Neisiany, S. Ramakrishna, *J. Appl. Polym. Sci.* **2019**, *136*, 47738.
[4] Y. Yang, Y. Du, J. Zhang, H. Zhang, B. Guo, *Adv. Fiber Mater.* **2022**, *4*, 1027.
[5] R. Dong, B. Guo, *Nano Today.* **2021**, *41*, 101290.
[6] I. S. Bayer, *Molecules* **2022**, *27*, 4504.
[7] M. Contardi, D. Russo, G. Suarato, J. A. Heredia-Guerrero, L. Ceseracciu, I. Penna, N. Margaroli, M. Summa, R. Spanò, G. Tassistro, L. Vezzulli, T. Bandiera, R. Bertorelli, A. Athanassiou, I. S. Bayer, *Chem. Eng. J.* **2019**, *358*, 912.
[8] T. A. Jeckson, Y. P. Neo, S. P. Sisinthy, B. Gorain, *J. Pharm. Sci.* **2021**, *110*, 635.
[9] S. B. Mahjour, X. Fu, X. Yang, J. Fong, F. Sefat, H. Wang, *Burns* **2015**, *41*, 1764.
[10] Z. Xie, C. B. Paras, H. Weng, P. Punnakitikashem, L. C. Su, K. Vu, L. Tang, J. Yang, K. T. Nguyen, *Acta Biomater.* **2013**, *9*, 9351.
[11] A. Choi, H. Kim, H. Han, J. H. Park, J. J. Kim, W. S. Sim, S. J. Lee, K. Ban, H. J. Park, D. S. Kim, *Biofabrication* **2022**, *15*, 015009.
[12] H. Han, H. Hong, S. M. Park, D. S. Kim, *Adv. Mater. Interfaces* **2020**, *7*, 2000571.
[13] H. Kim, J. Y. Lee, H. Han, W. W. Cho, H. Han, A. Choi, H. Hong, J. Y. Kim, J. H. Park, S. H. Park, S. W. Kim, D. S. Kim, D. W. Cho, *Sci. Rep.* **2021**, *11*, 9258.
[14] X. Zhao, B. Guo, H. Wu, Y. Liang, P. X. Ma, *Nat. Commun.* **2018**, *9*, 2784.
[15] Z. Li, A. Milionis, Y. Zheng, M. Yee, L. Codispoti, F. Tan, D. Poulikakos, C. H. Yap, *Nat. Commun.* **2019**, *10*, 5562.
[16] J. He, Y. Liang, M. Shi, B. Guo, *Chem. Eng. J.* **2020**, *385*, 123464.
[17] H. Zhang, X. Sun, J. Wang, Y. Zhang, M. Dong, T. Bu, L. Li, Y. Liu, L. Wang, *Adv. Funct. Mater.* **2021**, *31*, 2100093.
[18] W.-Y. Chen, H.-Y. Chang, J.-K. Lu, Y.-C. Huang, S. G. Harroun, Y.-T. Tseng, Y.-J. Li, C.-C. Huang, H.-T. Chang, *Adv. Funct. Mater.* **2015**, *25*, 7189.
[19] N. C. Cady, J. L. Behnke, A. D. Strickland, *Adv. Funct. Mater.* **2011**, *21*, 2506.
[20] H.-J. Eom, J. Choi, *Environ. Sci. Technol.* **2010**, *44*, 8337.
[21] X. Lan, Y. Liu, Y. Wang, F. Tian, X. Miao, H. Wang, Y. Tang, *Int. J. Pharm.* **2021**, *601*, 120525.
[22] L. A. Schneider, A. Korber, S. Grabbe, J. Dissemond, *Arch. Dermatol. Res.* **2007**, *298*, 413.
[23] R. Rahimi, M. Ochoa, T. Parupudi, X. Zhao, I. K. Yazdi, M. R. Dokmeci, A. Tamayol, A. Khademhosseini, B. Ziaie, *Sens. Actuators, B* **2016**, *229*, 609.
[24] A. Nocke, A. Schröter, C. Cherif, G. Gerlach, *Autex Res. J.* **2012**, *12*, 20.
[25] S. Han, Y. Yang, *Dyes Pigm.* **2005**, *64*, 157.
[26] A. E. Krausz, B. L. Adler, V. Cabral, M. Navati, J. Doerner, R. A. Charafeddine, D. Chandra, H. Liang, L. Gunther, A. Clendaniel, S. Harper, J. M. Friedman, J. D. Nosanchuk, A. J. Friedman, *Nanomedicine* **2015**, *11*, 195.
[27] N. Pan, J. Qin, P. Feng, Z. Li, B. Song, *J. Mater. Chem. B* **2019**, *7*, 2626.
[28] B. Kuswandi, Jayus, T. S. Larasati, A. Abdullah, L. Y. Heng, *Food Anal. Methods* **2012**, *5*, 881.
[29] Z. Su, H. Ma, Z. Wu, H. Zeng, Z. Li, Y. Wang, G. Liu, B. Xu, Y. Lin, P. Zhang, X. Wei, *Mater. Sci. Eng. C* **2014**, *44*, 440.
[30] T. G. Sahana, P. D. Rekha, *Mol. Biol. Rep.* **2018**, *45*, 2857.
[31] E. Proksch, R. de Bony, S. Trapp, S. Boudon, *J. Dermatol. Treat.* **2017**, *28*, 766.
[32] Z. Stanić, *Plant Foods Hum. Nutr.* **2017**, *72*, 1.
[33] J. Li, A. He, C. C. Han, D. Fang, B. S. Hsiao, B. Chu, *Macromol. Rapid Commun.* **2006**, *27*, 114.
[34] R. N. Wenzel, *Ind. Eng. Chem.* **1936**, *28*, 988.
[35] International Standards Organization, ISO 9237, **1995**.
[36] A. B. D. Cassie, S. Baxter, *Trans. Faraday Soc.* **1944**, *40*, 546.
[37] S. Michielsen, H. J. Lee, *Langmuir* **2007**, *23*, 6004.

© 2023 Wiley-VCH GmbH

2365709x, 2023, 7, Downloaded from https://onlinelibrary.wiley.com/doi/10.1002/admt.202201765 by Korea Advanced Institute Of, Wiley Online Library on [10/08/2023]. See the Terms and Conditions (https://onlinelibrary.wiley.com/terms-and-conditions) on Wiley Online Library for rules of use; OA articles are governed by the applicable Creative Commons License